



## Exploration of Periodic Flow Fields

Allen R. Sanderson<sup>1,c</sup>, Xavier Tricoche<sup>2</sup>

<sup>1</sup>Scientific Computing and Imaging Institute, University of Utah, Salt Lake City, UT 84112, USA

<sup>2</sup>Computer Graphics and Visualization Laboratory, Purdue University, West Lafayette, IN 47907, USA

<sup>c</sup>Corresponding author: Telephone.: +1.801.585.0769; Email:allen@sci.utah.edu

### KEYWORDS:

**Main subjects:** flow visualization

**Fluid:** transport

**Visualization method(s):** Poincaré Plot, Finite-Time Lyapunov Exponents

**Other keywords:** dynamical systems, periodic flows

**ABSTRACT:** *One of the difficulties researchers face when exploring flow fields is understanding the respective strengths and limitations of the visualization and analysis techniques that can be applied to their particular problem. We consider in this paper the visualization of doubly periodic flow fields. Specifically, we compare and contrast two traditional visualization techniques, the Poincaré plot and the finite-time Lyapunov exponent (FTLE) plot with a technique recently proposed by the authors, which enhances the Poincaré plot with analytical results that reveal the topology. As is often the case, no single technique achieves a holistic visualization of the flow field that would address all the needs of the analysis. Instead, we show that additional insight can be gained from applying them in combination.*

### 1 Introduction

One of the difficulties researchers face when exploring flow fields is understanding the respective strengths and limitations of the flow visualization and analysis techniques that can be utilized for their particular application. In this paper, we consider techniques that can be applied to flow fields that are doubly periodic. Two examples are toroidal magnetic fields [1] and rotating cylindrical flow fields [2]. These flow fields are periodic in the toroidal and poloidal directions and are form a Hamiltonian system [4]. In magnetic confinement fusion reactors, (e.g., tokamaks), toroidal magnetic fields are used to confine a burning plasma. A rotating cylinder flow field on the other hand has a vertical overturning and horizontal swirling motion and is an idealization of motion observed in ocean eddies.

When these fields are perturbed by a symmetry breaking disturbance, chaos arises. Some trajectories survive the perturbation and act as barriers to chaotic transport, a result consistent with an extension of the KAM theorem for three-dimensional, volume-preserving flow [4]. Understanding the development and breakdown of these fields is a critical research component in fusion reactor design and in the study of ocean transport, respectively.

In this paper, we compare and contrast two traditional visualization techniques, namely the puncture plot (*i.e.*, Poincaré map [3]) and the finite-time Lyapunov exponent (FTLE) plot [5,6] with a recently developed technique, the enhanced puncture plot, which allows for visualization and analysis [7,8]. As our primary focus is on comparing these visualization techniques, the reader is here referred to [3-8] to for more technical details.

## 2 Methods

The simplest way to explore a doubly periodic system that is topologically a torus with a major and minor axis is to create a puncture plot. To create such a plot, one defines a plane  $\Sigma$  perpendicular to the major axis. Next one selects a series of initial conditions (or seed points) on from which trajectories (integral curves) are computed. The seeds are typically uniformly spaced along a line in the plane rather than on a 2D grid because for quasi-periodic Hamiltonian systems integral curves are typically volume filling. The successive intersections of the trajectories with the puncture plane (i.e. the Poincaré map) forms the puncture plot, Figure 1.

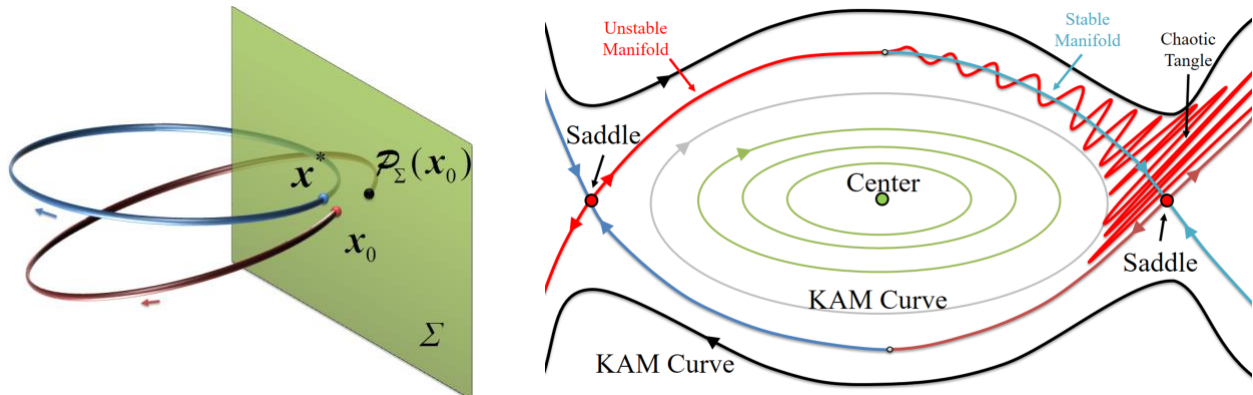


**Figure 1. Poincaré map.** Left: Transverse plane and trajectories. Right: Topological structures associated with a Poincaré map in a so-called near-integrable dynamical system, such as those considered in this paper.

Creating a puncture plot is simple and only requires an accurate integration scheme and a fast puncture test. However, though the integral curves are volume filling, there is no guarantee that the complete volume will be sampled during the chosen finite number of integration steps thus structures may be missed. Further, the formation of structures is highly dependent on trajectory length (i.e., the number of integration steps). As such, structures may not be properly revealed if too few integration steps are taken. Despite these drawbacks, it is the predominant tool used to explore periodic flow fields.

Another technique often used to explore flow fields is to plot the finite-time Lyapunov exponent (FTLE) for a trajectory [5,6]. The FTLE is a scalar value that represents the rate of separation of infinitesimally close trajectories. Similar to the puncture plot, for doubly periodic systems the FTLE plot can be combined with dimension reduction since it suffices to consider its restriction to a plane perpendicular to the major axis. However, unlike the puncture plot which relies on a small number of trajectories to form the flow map, the FTLE plot is computationally expensive because it requires a large number of trajectories to densely construct the flow map.

One of the problems that must be addressed when calculating FTLE is the choice of spatial discretization. While the FTLE plot can show the overall large-scale structures, very fine details can be hard to discern or will be missed entirely unless a finer grid is used. Further, we follow the process described by Onu [6] and utilize an auxiliary grid to achieve an increase in accuracy of the finite difference approximation used in the computation of the derivative of the Cauchy-Green strain tensor. However, increasing the sampling resolution and using an auxiliary grid

come with a greater computational cost [9]. Owing to the chaotic nature of the systems being explored many structures will be obfuscated by aliasing artifacts and therefore are hard to discern.

One of the deficiencies with both the Poincaré and FTLE plots is that they do not permit any direct quantitative analysis of the periodicity within the flow field, specifically, the toroidal and poloidal periodicity. However, Lagrangian coherent structures (LCS) such as shrink (repelling LCSs) and stretch lines (attracting LCSs) can be extracted using techniques described by Onu [6].

Recently, the authors proposed a technique that while adaptively creating a Poincaré plot analyzes the trajectory and determines among other characteristics, the toroidal and poloidal periodicity of the trajectory [7,8]. Subsequent analysis of the periodicity can then be used to determine whether the trajectory is rational, irrational, or forms an island chain. If the fundamental periods are equal to the toroidal and poloidal periods, the trajectory lies on a rational or irrational surface, whereas if the fundamental periods are proportional to the toroidal and poloidal periods, the trajectory lies on an island chain [8]. Topologically, an island chain is a series of homoclinic connections between the successive return points of a hyperbolic periodic orbit. This quantitative analysis is used to create an enhanced Poincaré plot which allows insightful cross sectional profiles to be generated using a small number of puncture points. That is the profile consists of a series of line segments based on a small number of puncture points. In contrast, a traditional Poincaré plot relies on a large number of puncture points to imply a cross sectional profile.

## Results

We compare and contrast these three techniques for visualization and demonstrate how the analysis aids in the understanding of the flow map. Each technique represents a compromise between responsiveness and interactivity on one hand, and detailed and precise analysis on the other hand.

In this investigation, we consider two practical cases of Hamiltonian dynamical systems with two degrees of freedom, namely toroidal magnetic fields and rotating cylindrical flow fields [4]. The first example stems from a simulation of the disruption of the magnetic field in the DIII-D tokamak [1,10] where physicists were interested in the breakup of the magnetic field and the subsequent loss of confinement of the burning plasma. The second example corresponds to a simulation of chaotic advection within a steady, three-dimensional, Ekman-driven, rotating cylinder flow, where oceanographers study the formation of ocean mesoscale and submesoscale eddies [2]. In both cases, the simulation utilizes a high-resolution grid composed 2D Lagrange-type finite elements, and finite Fourier series [11] or 3D spectral elements [12], respectively.

Each of the three techniques discussed previously were implemented as part of the VisIt toolkit using the *Parallel Integral Curve System* (PICS) [13,14]. The PICS system allows for massively parallel computation of integral curves using a variety of integration methods. The Adams-Bashforth method was selected because of its accuracy and its use of a fixed step length, which is important because the periodicity analysis requires dense sampling along the integral curve. Though the PICS systems supports the integration of time-varying flow fields, in both examples we restrict our considerations to the steady state integral curves and surfaces that are formed. In

the visualization vernacular, steady state integral curves are referred to as *streamlines*, whereas time-dependent integral curves are referred to as *pathlines*.

As an introduction to the first case, we show the contrast in the complexity of stochastic and non-stochastic integral curves as they traverse through the steady state flow field from [2], Figure 2. The corresponding Poincaré plot used  $\sim 100$  seed points and clearly shows surfaces and islands chains in both the non-stochastic and stochastic regions, Figure 3. Such plots are the de facto standard because of the ease of their construction. However, because the color mapping is based on the seed point's unique identifier, disambiguating between adjacent surfaces can be difficult.

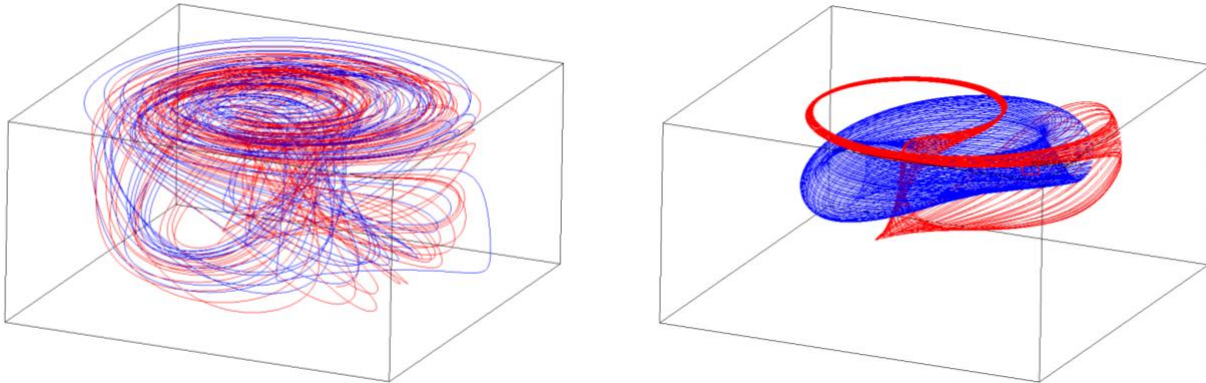


**Figure 2.** An example of the complexity of two stochastic (left) and non-stochastic (right) integral curves as they traverse through the steady state flow field from [2].

A FTLE plot was then constructed using a  $400 \times 400$  grid of seed points equally spaced throughout the domain in the X-Z plane using a 3D auxiliary grid as described by Onu [6]. The auxiliary grid was comprised of six points placed symmetrically around each seed point. Though the FTLE plot is being constructed the X-Z plane, for a 3D auxiliary grid was used because the trajectories are 3D. Though not shown, utilizing a 2D grid results in artifacts. The resulting FTLE plot required 960K points with 200K integration steps, Figure 5. The FTLE plot clearly shows the stochastic regions as a noise pattern with many seemingly organized structures within it. Conversely, there are artifacts due to the somewhat coarse sampling density that appear as moray patterns.

If we compare the sparse Poincaré plot with the dense FTLE plot, it is obvious that the number of seed points utilized is clearly the dominating parameter. For instance, in the lower left corner is a complex island chain. Visible in Poincaré plot are both primary and secondary island chains (a secondary island chain is one that surrounds, or is surrounded by a primary island chain). Though the FTLE plot makes it much harder to discern these structures, the locations of fixed points (*e.g.*, O-points) where the flow is truly periodic can be seen in the small Lyapunov exponent values. In the Poincaré plot, shown in blue within the green region, are a series of islands that appear to be part of the stochastic region, in the FTLE plot. This difference can be attributed to the time scale selected for calculating the Lyapunov exponent, which was probably too long.

Next, the enhanced Poincaré plot was constructed using the same seed points used for the standard Poincaré plot for Figure 3, Figure 5. Though not necessary, puncture points (opposed to

cross sectional profiles based on a small number of puncture points) are utilized in order to enable a more direct comparison to the Poincaré plot. The enhanced Poincaré plot also clearly shows surfaces and islands chains in both the non-stochastic and stochastic regions. Like the Poincaré plot, it too suffers from being difficult to disambiguate between adjacent surfaces due to the color mapping choice which is based on the ratio of the toroidal to poloidal periodicity.

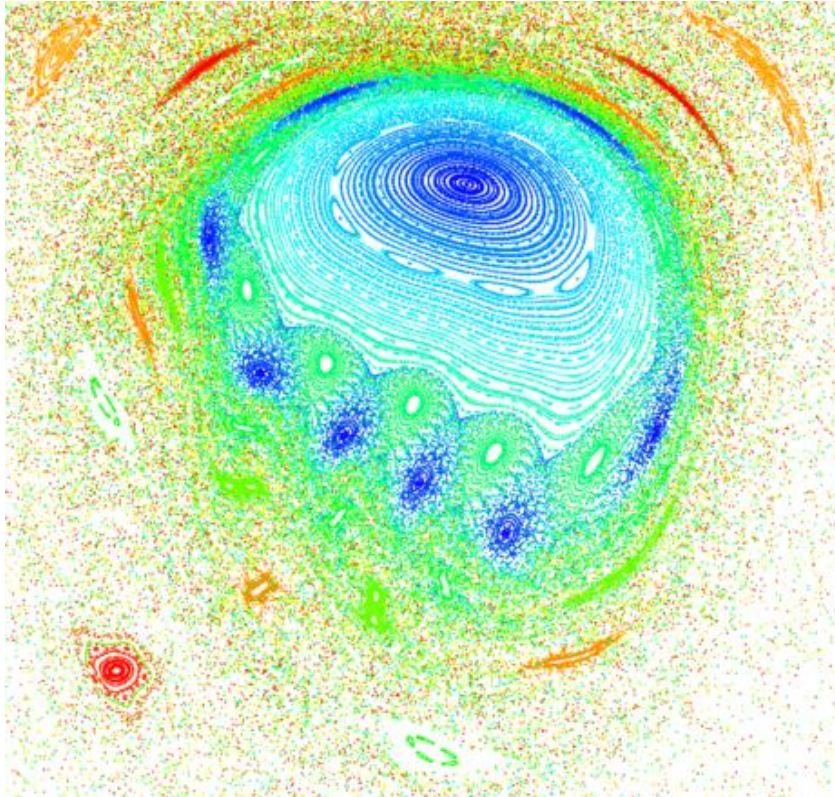


**Figure 3.** A Poincaré plot for a steady, three-dimensional, Ekman-driven, rotating cylinder flow, colored based on the seed point's unique identifier.

However, unlike the Poincaré plot and the FTLE plot, the enhanced Poincaré plot contains the results of the trajectory analysis including the toroidal and poloidal periodicity as well as the correspondence between island chains. This correspondence allows approximate cross sectional profiles to be reconstructed by connecting neighboring puncture points into a series of line segments, Figure 6. The cross-sectional profile is approximate because a series of linear line segments are used. As a final step to demonstrate the utility of determining the correspondence between puncture points, the 2,1 island chain and the quasi-periodic surface from Figure 2 (right) are reconstructed in 3D, Figure 8. This 3D reconstruction and coloring is based on the puncture point ordering and shows the twisting complexity of the surfaces. Such 3D reconstructions are not otherwise possible with images such as that in Figure 2 (right) being the norm.

The second case presented is from a magnetic confinement fusion simulation of the dynamics of the major disruption of DIII-D discharge 87009 [1]. In this case, the magnetic field is represented as a time varying vector field with the instantaneous field being of interest. A Poincaré plot is first constructed using 108 seed points (three lines of 36 points each) and clearly shows surfaces and islands chains in both the non-stochastic and stochastic regions, Figure 9 (left). The zoomed

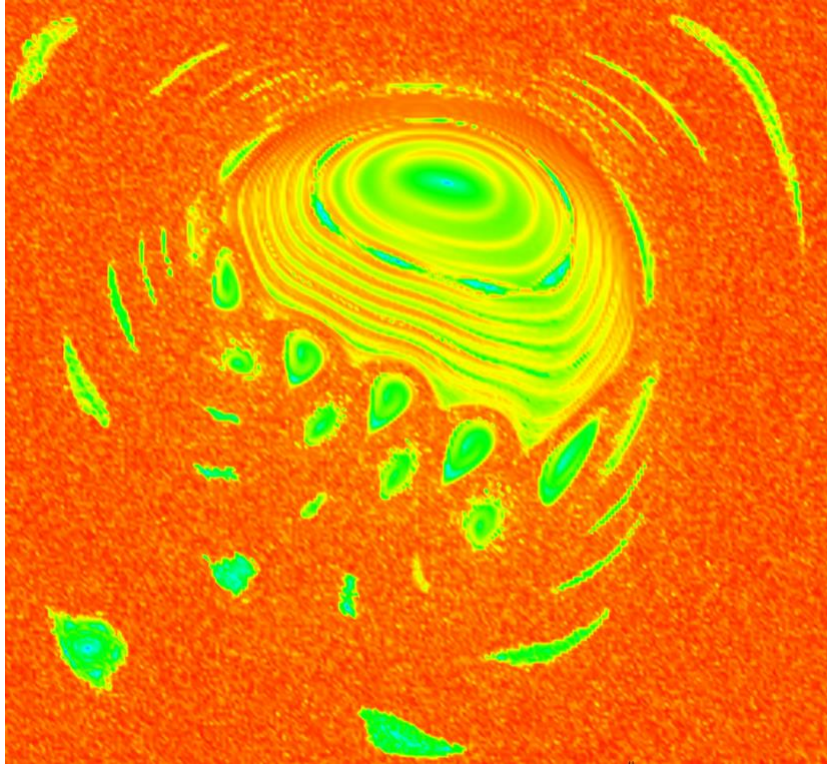


**Figure 4.** *The FTLE plot for same simulation in Figure 2 using a 400x400 grid of seed points and a 3D auxiliary grid color based on the largest Lyapunov exponent.*

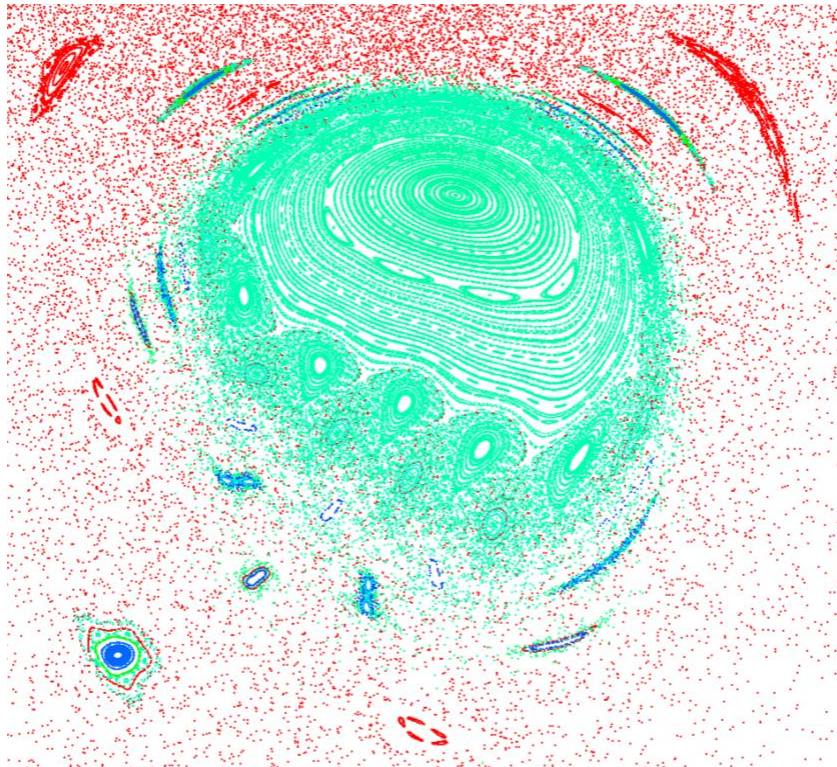


**Figure 5.** *The enhanced Poincaré plot for same simulation in Figure 2 colored based on the ratio of the toroidal to poloidal windings.*

image shows even more details into the complexity of two different islands chains, Figure 9 (right). The overall quality of the Poincaré plot demonstrates why such plots are the de facto standard for post-hoc analysis within the Fusion community.

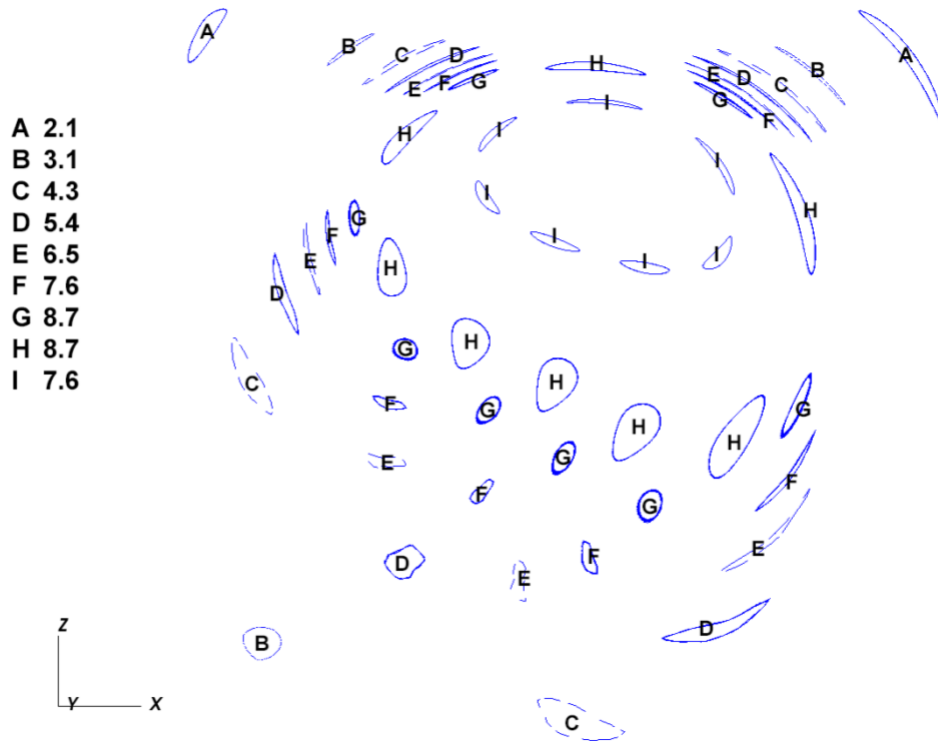


**Figure 6.** An example of an enhanced Poincaré plot for same simulation in Figure 2 with the major island chains identified along with the ratio of their toroidal to poloidal windings. Note: the labels were manually added to the plot based on the analysis results.

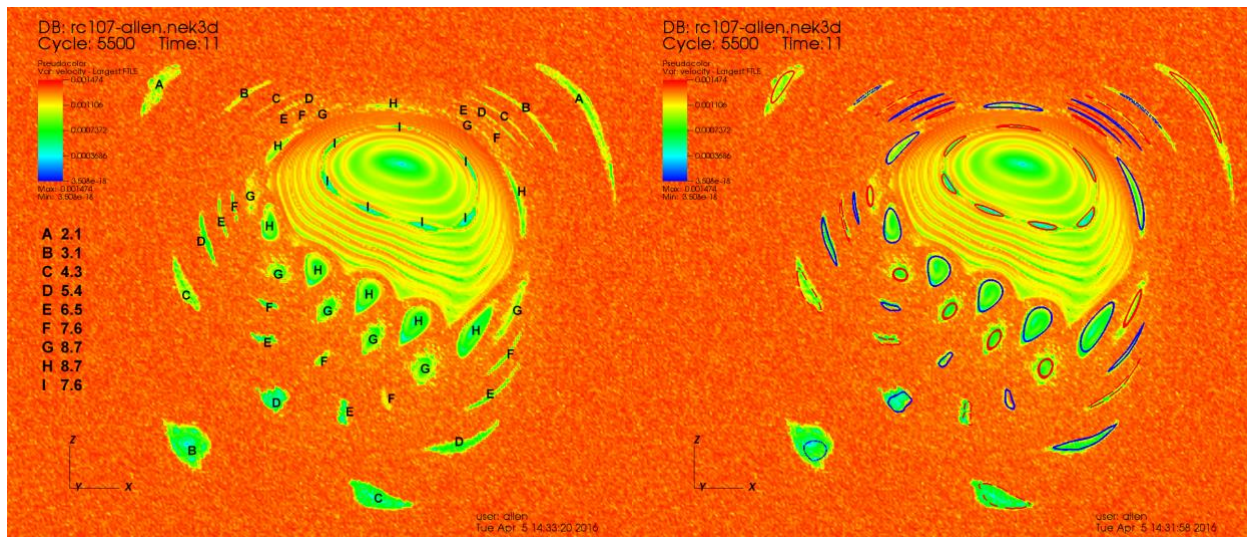


**Figure 7.** An overlay of the enhanced Poincaré plot onto the FTLE plot from Figure 4 showing the major island chains. Note: the labels were manually added to the plot based on the analysis results.

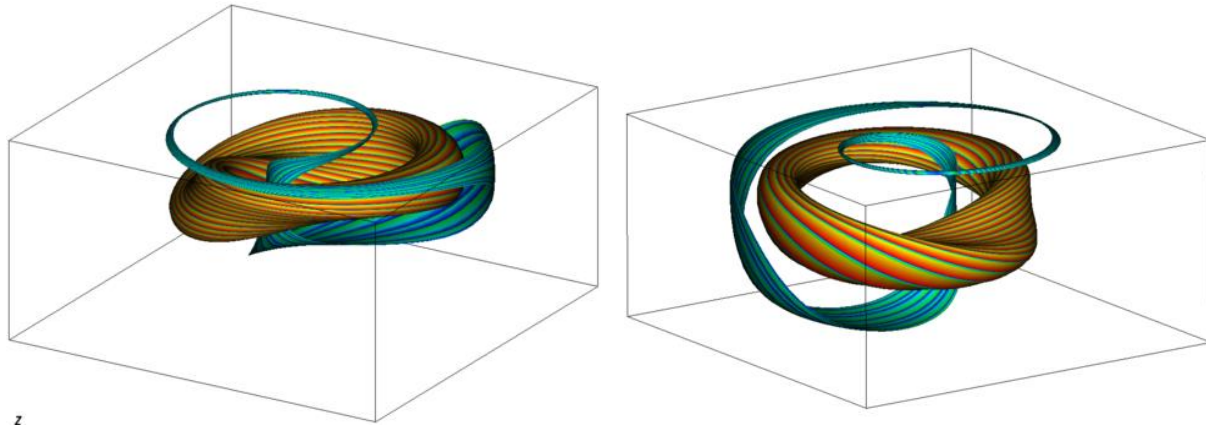


**Figure 8.** From Figure 2 (right) a three-dimensional surface reconstruction of the 2,1 island chain labeled as "A" in Figure 6 (green-blue) and the quasi-periodic surface (yellow-red). The left perspective corresponds to the same perspective in Figure 2 (right).

A FTLE plot was then constructed using a  $913 \times 1753$  grid of seed points equally spaced throughout the domain in the X-Z plane using a 3D auxiliary grid comprised of six points placed symmetrically around each seed point. The resulting FTLE plot utilized 9.6M points with 66.7K integration steps, Figure 10. The FTLE plot clearly shows the stochastic regions as a noise pattern with many organized structures within it as well as the interior. Overall the quality of the plot is quite high but as noted the computational expense is also quite high, 1200 ranks were used over a 10 hour time period.

Next, the enhanced Poincaré plot was constructed using 43 seed points (36 points from traditional Poincaré plot and seven additional points). This plot also clearly shows surfaces and islands chains in both the non-stochastic and stochastic regions, Figure 11. Unlike the traditional Poincaré plot where a of series of points are used to infer the cross-sectional profile, the enhanced Poincaré plot analysis provides correspondence between puncture points which allows the cross-sectional profile of each surface to be represented as a series of line segments. This representation provides a cleaner visualization but in some cases at a cost when too few points are available to construct the line segment and results in long linear segments.

We next overlay the enhanced Poincaré plot from Figure 11 (right) on to the FTLE plot from Figure 10 (right) and include the toroidal and poloidal periodicity of the trajectory analysis as well as label the island chains, Figure 12. For the 3,1 island chain, it contains two secondary chains, 18,6 and 15,3, both of which have the same ratio as the 3,1 island chain and how they are differentiated from rational and irrational surfaces. The final step again demonstrates the utility of the correspondence between puncture points by reconstructing three islands chains in 3D, Figure 13.

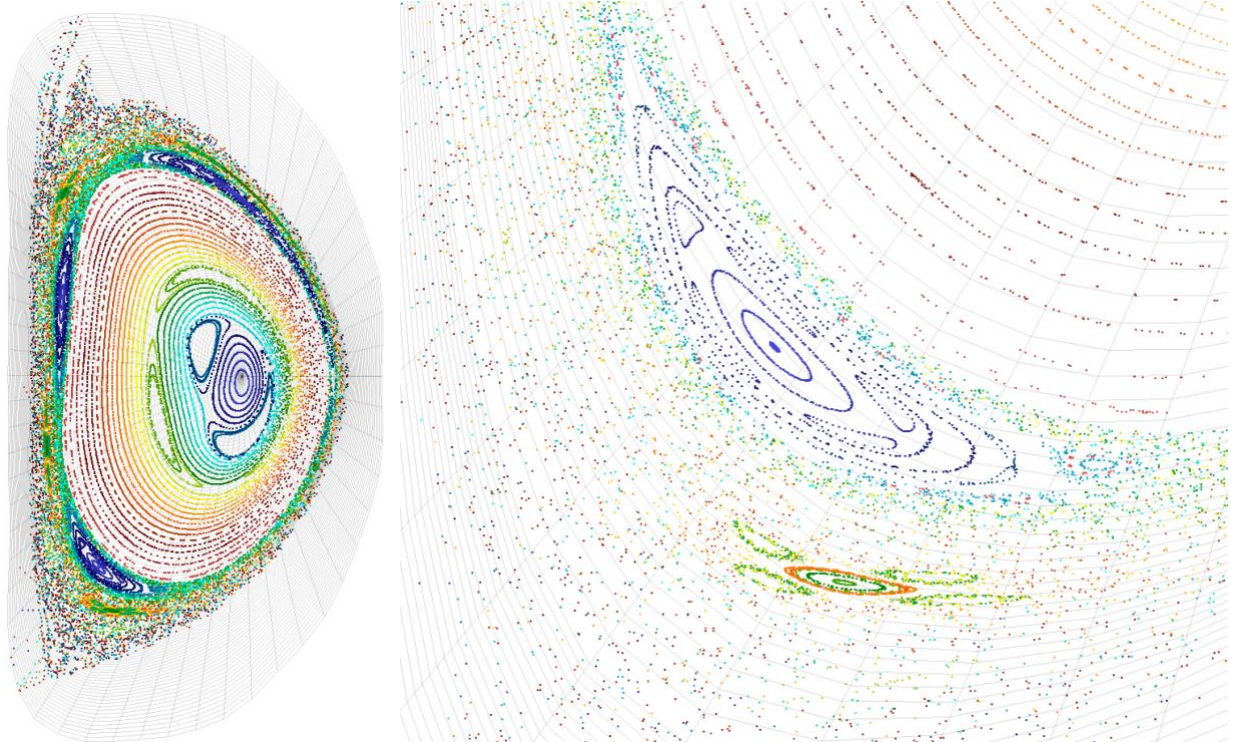


**Figure 9.** A Poincaré plot of magnetic field from the major disruption of DIII-D discharge 87009 colored based on the seed point ordering. The left image shows the complete plot, the right image shows a zoomed view of the lower inboard side.

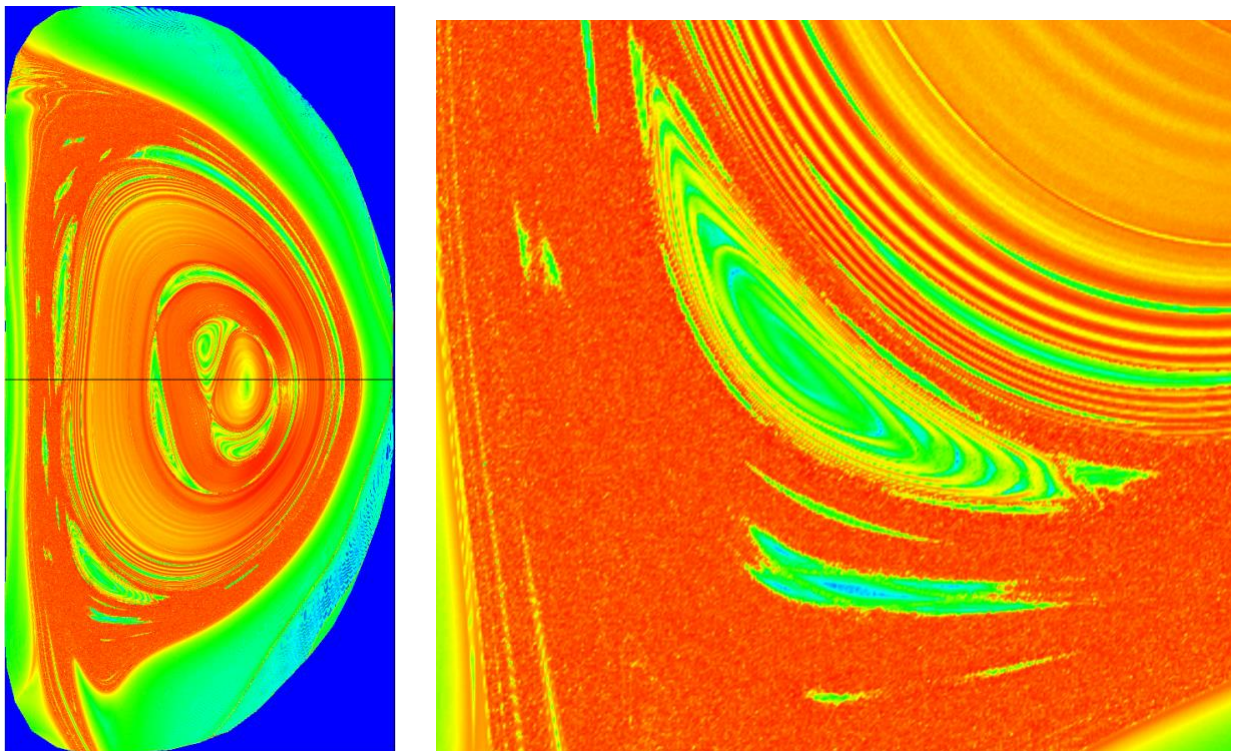


**Figure 10.** The FTLE plot for same simulation in Figure 9 using a  $913 \times 1753$  grid of seed points and a 3D auxiliary grid colored based on the largest Lyapunov exponent.

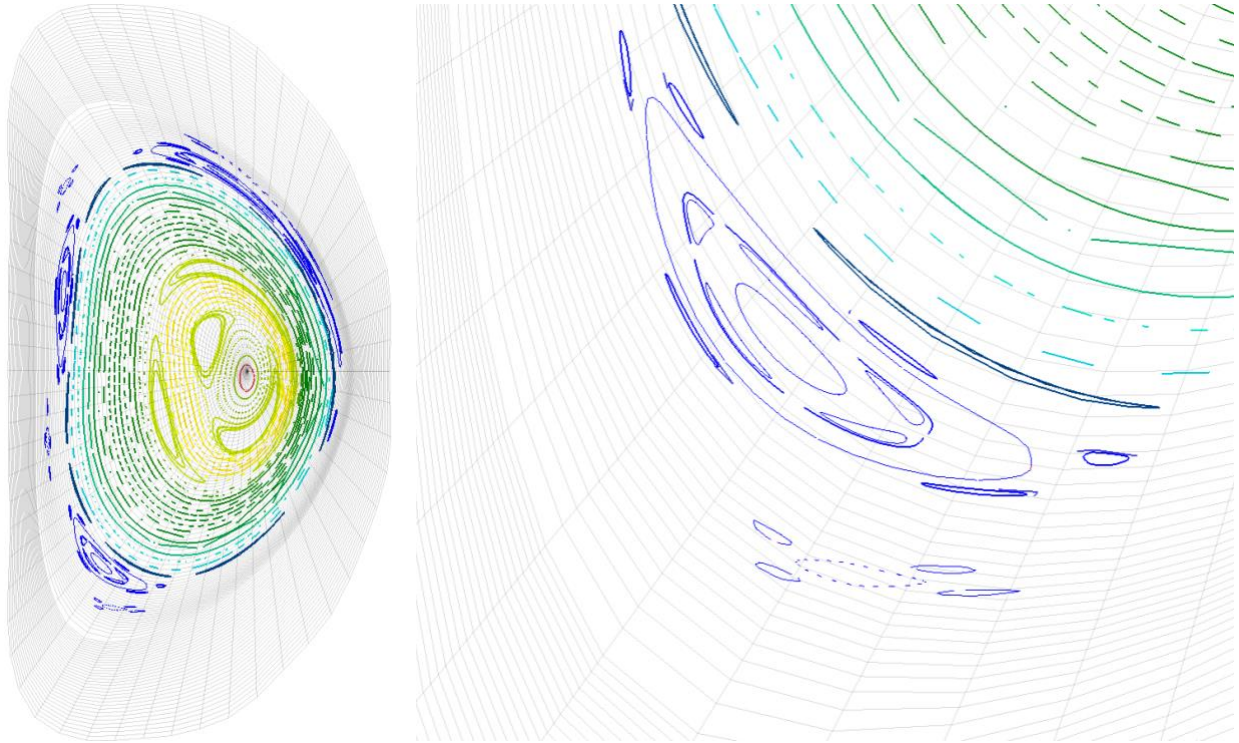


**Figure 11.** The enhanced Poincaré plot for same simulation in Figure 9 colored based on the ratio of the toroidal to poloidal windings.

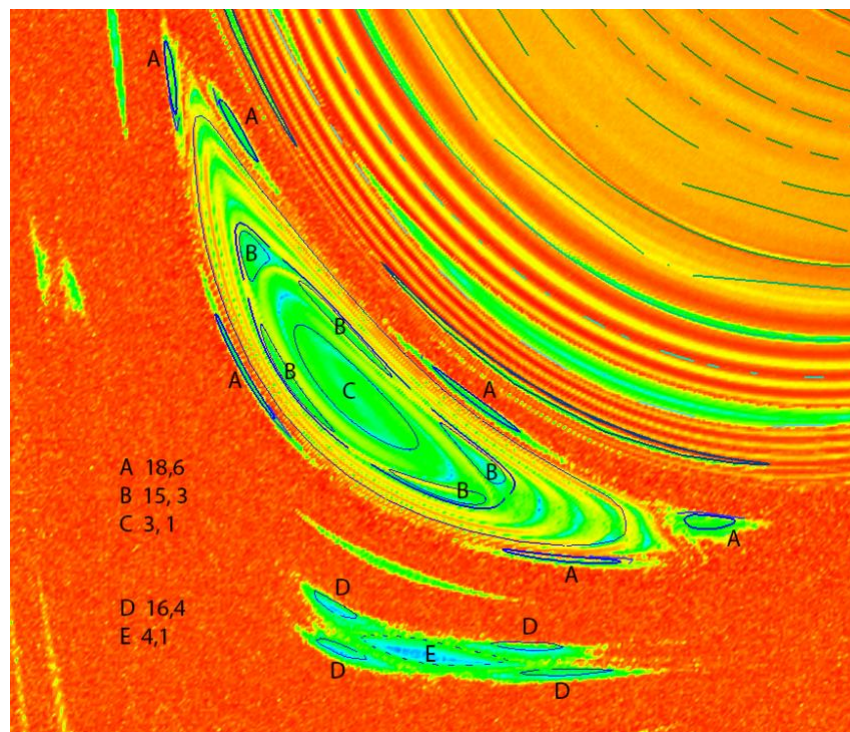


**Figure 12.** An overlay of the enhanced Poincaré plot onto the FTLE plot with the island chains labeled. Island chains C and E are primary islands, while A, B, and D are secondary islands. Note: the labels were manually added to the plot based on the analysis results.

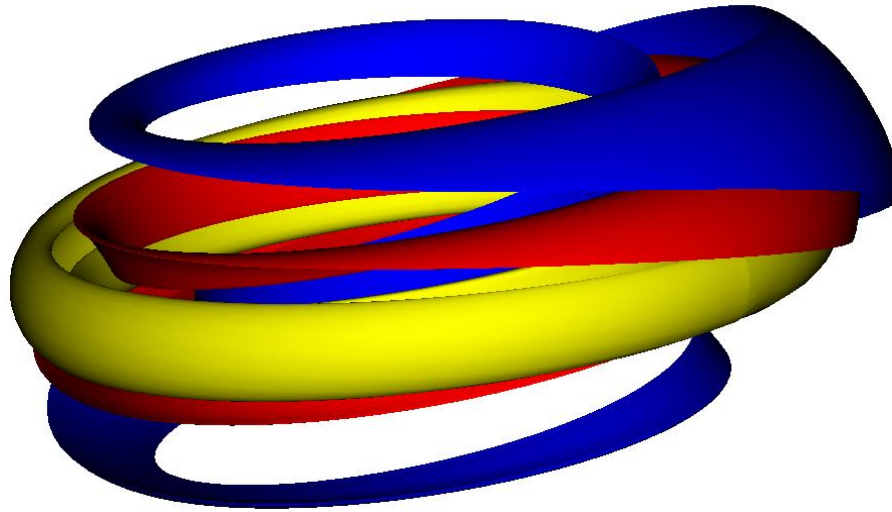


**Figure 13.** A three-dimensional surface reconstruction of the two 2,1 island chains (red, yellow) and the 3,1 island chain (blue) labeled as "C" in Figure 12.

### Discussion

Each of the three techniques presented provide similar and different details. The traditional Poincaré plots are computationally cheap and quickly provide useful information. Though computationally cheap, resources can be wasted because of duplicate puncture points that are generated from similar seed locations and excessive integration. Even with the sparse point density and the inherent discontinuous nature of such plots which may hide or otherwise make it difficult to perceive features, they are the de facto standard for periodic systems.

FTLE plots on the other hand are computationally expensive to calculate. The FTLE images shown took on the order of hours utilizing 200-1000 processors running in parallel (the integration is embarrassingly parallel when the full domain can be loaded into memory on each processor). The number of integration steps is critical for visualizing features especially as the FTLE is being calculated for a steady state or instantaneous point in time. Despite these drawbacks their continuous nature is a highly desirable feature.

The enhanced Poincaré plots lie between the traditional Poincaré plots and the FLTE plots. They are slightly more computationally expensive to generate than a traditional Poincaré plot, taking minutes rather than seconds to generate. Though not continuous they are not discrete either. Like the traditional Poincaré plot they can suffer from too few seed locations and missed features. However, because it is possible to reconstruct the cross-sectional profile by obtaining a series of line segments using techniques developed for streamline placement to obtain evenly spaced cross sections may be applicable [15]. However, unlike both the traditional Poincaré plot and FTLE plot the enhanced Poincaré plot contains a rich set of analysis data that can be utilized. Such analysis data goes beyond the data extracted from FLTE plots in [6] for limit cycles and shrink and stretch lines as it can be utilized for reconstructing surfaces and lends itself to being utilized within a running simulation. Though not shown, it has been our experience that the analysis performs well before the system becomes highly stochastic after which the analysis defaults to a traditional Poincaré plot output.

Finally, we should note that constructing the plots was an iterative process. That is because the tools were meant to be used interactively. For instance, the traditional and enhanced Poincaré plots were created as an initial visualization which were then explored in more detailed when features were found. Because of the computational expense, FTLE plots were generated for a small region of interest using the Poincaré plots as a guide. Once an acceptable resolution and other parameters were found, a plot of the complete plane was generated.

## Conclusion

As is often the case, no single technique achieves a holistic visualization of the flow field that would address all the needs of the analysis. In this work, we discussed the respective strengths and limitations of three visualization techniques for periodic flow phenomena and document the additional insight that can be gained from applying them in combination.

## References

- [1] S. Kruger, D. Schnack, and C. R. Sovinec. Dynamics of the major disruption of a diii-d plasma. *Phys. Plasmas*, 12:56113, 2005.
- [2] L. Pratt, I. Rypina, T.M. Özgökmen, P. Wang, H. Childs and Y. Bebieva, “Chaotic advection in a steady, three-dimensional, Ekman-driven eddy,” *Journal of Fluid Dynamics*, 738, pp. 143-183, 2014.
- [3] H. Poincaré, *Oeuvres de Henri Poincaré*. Gauthier-Villars, Paris, 1934-65.
- [4] V. I. Arnold, “Proof of a Theorem of A.N. Kolmogorov on the Invariance of Quasiperiodic Motions Under Small Perturbations of the Hamiltonian.” *Russ. Math. Surveys* 18:5: pp. 9-36, 1963.
- [5] G. Haller and T. Sapsis. Lagrangian coherent structures and the smallest finite-time Lyapunov exponent, *CHAOS* 21, 023115, 2011.
- [6] K. Onu, F. Huhn, & G. Haller, LCS Tool: A Computational platform for Lagrangian coherent structures, *J. of Computational Science*, 7 pp. 26-36, 2005.
- [7] A.R. Sanderson, G. Chen, X. Tricoche, D. Pugmire, S. Kruger, J. Breslau. “Analysis of Recurrent Patterns in Toroidal Magnetic Fields,” In *IEEE Transactions on Visualization and Computer Graphics*, Vol. 16, No. 6, IEEE, pp. 1431-1440. Nov, 2010.
- [8] A.R. Sanderson, G. Chen, X. Tricoche, E. Cohen. “Understanding Quasi-Periodic Fieldlines and Their Topology in Toroidal Magnetic Fields,” In *Topological Methods in Data Analysis and Visualization II*, Edited by R. Peikert and H. Carr and H. Hauser and R. Fuchs, Springer, pp. 125--140. 2012.
- [9] X. Tricoche, C. Garth, A. Sanderson. “Visualization Invariant Manifolds in Area-Preserving Maps,” In *Topological Methods in Data Analysis and Visualization II*, Edited by R. Peikert and H. Carr and H. Hauser and R. Fuchs, Springer, pp. 109-124, 2012.
- [10] DIII-D "<https://fusion.gat.com/global/diii-d/home>". Retrieved May 1, 2018.
- [11] C.R. Sovinec, A.H. Glasser, D.C. Barnes, T.A. Gianakon, R.A. Nebel, S.E. Kruger, D.D. Schnack, S.J. Plimpton, A. Tarditi, M.S. Chu and the NIMROD Team, "Nonlinear Magnetohydrodynamics with High-order Finite Elements," *Journal of Computational Physics*, 195, 355 (2004).
- [12] FISCHER, P. F. 1997 “An overlapping Schwarz method for spectral element solution of the incompressible Navier–Stokes equations”. *J. Comput. Phys.* 133, 84–101.
- [13] H. Childs, E. Brugger, B. Whitlock, J. Meredith, S. Ahern, D. Pugmire, K. Biagas, M. Miller, C. Harrison, G. H. Weber, H. Krishnan, T. Fogal, A. Sanderson, C. Garth, E. W. Bethel, D. Camp, O. R. ubel, M. Durant, J. M. Favre, and P. Navratil. VisIt: An End-User Tool For Visualizing and Analyzing Very Large Data. In *High Performance Visualization - Enabling Extreme-Scale Scientific Insight*, pages 357-372. CRC Press, Oct 2012.
- [14] D. Pugmire, H. Childs, C. Garth, S. Ahern, and G. Weber. 2009. “Scalable computation of streamlines on very large datasets”. In *Proceedings of the Conference on High Performance Computing Networking, Storage and Analysis (SC '09)*.
- [15] Z. Liu, R. Moorhead, and J. Groner, “An Advanced Evenly-Spaced Streamline Placement Algorithm,” *IEEE Transactions on Visualization and Computer Graphics*, 12(5):965-72.

### **Copyright Statement**

The authors confirm that they, and/or their company or institution, hold copyright on all the original material included in their paper. They also confirm they have obtained permission, from the copyright holder of any third-party material included in their paper, to publish it as part of their paper. The authors grant full permission for the publication and distribution of their paper as part of the ISFV18 proceedings or as individual off-prints from the proceedings.